JOURNAL OF IMAGING SCIENCE AND TECHNOLOGY® • Volume 48, Number 3, May/June 2004

Crosslinkable Branched Hydrazones as Hole Transporting Materials

V. Getautis,* O. Paliulis and I. Paulauskaite
Faculty of Chemical Technology, Kaunas University of Technology, Kaunas, Lithuania

V. Gaidelis and V. Jankauskas
Department of Solid State Electronics, Vilnius University, Vilnius, Lithuania

J. Sidaravicius
Department of Polygraphic Machines, Vilnius Gediminas Technical University, Vilnius, Lithuania

Z. Tokarski,▲ K. Law▲ and N. Jubran▲
Samsung Information Systems America, Digital Printing Solutions Laboratory, Woodbury, Minnesota, USA

The new hole transport materials which comprise molecules consisting of two hydrazone branches linked by a central bridge containing a flexible thiophenyl sulfide and two hydroxyl groups were synthesized and investigated. These transporting materials are low molecular weight glasses and allow preparation of layers stable to crystallization. Ionization potential of the materials is in the range 5.03–5.38 eV. The highest hole mobility, reaching 10^{-4} cm^2/Vs at 6×10^5 V/cm electric field, was observed in the transport material with dimethyltriphenylamine or triphenylamine moieties. These transport materials can be used with or, in the case of a solid substrate, without polymer binder. They can be chemically crosslinked in the layer by reaction of the hydroxyl groups with polyisocyanates.

Journal of Imaging Science and Technology 48: 265–272 (2004)

Introduction

Aromatic hydrazone molecules dispersed in a binder polymer are used as the main constituent of electrophotographic devices due to their excellent hole transporting properties and relatively simple synthesis.[1–4] The presence of large proportion of binder in the electrophotographic layers (EPL), usually 50% of the total composition mass leads to considerable decrease of carrier mobility. Even in such compositions, possibility of the transport material (TM) crystallization remains and causes problems during EPL preparation and long-term application, because low molecular weight hydrazones generally tend to form crystals. It is of interest and significance to develop photo- and electroactive low molecular weight amorphous materials that form stable amorphous glasses having glass transition temperatures above room temperature. These molecular glasses will form stable films without a binder, and are expected to manifest properties and functions more effectively than molecularly doped polymer compositions. Among the great number of studies devoted to low molar mass aromatic hydrazones only few glass-forming compounds with the hydrazone moiety are reported.[5–8] Another problem, which arises with preparation of the belt format EPL on flexible supports, involves bending and stretching stability of the layers. This problem is especially acute in the machines with liquid development, because liquid developer promotes crack formation. Solving these problems requires new TM with special molecule design and improved properties.

We have reported on novel class of well defined molecular glasses, obtained by the reaction of oxiranes containing photoconductive groups with different bifunctional compounds, such as aromatic diols, dimercapto compounds, and derivatives of aniline.[9–11] The existence of several diastereoisomers, the possibility of intermolecular hydrogen bonding and flexibility of aliphatic linking chains ensure high morphological stability of these glasses. In the present article we report on new, branched hydrazone derivatives as hole transport materials. The molecules of these TM consist of two hydrazone branches linked by a central, flexible thiophenyl sulfide containing bridge. The molecular structure of these TM makes crystallisation in solid state difficult, so these materials are low molecular weight glasses. Another feature of these TM is presence of two

---

Original manuscript received August 5, 2003

▲ IS&T Member

* vgetaut@ktu.lt

hydroxyl groups in the molecule. This improves adhesion and compatibility with various binders, including polycarbonate (PC) and polyvinylbutyral (PVB). These TM can then be used without binder in the case of solid substrate or with binder in low concentrations. They can be chemically crosslinked in the layer by reaction of the –OH groups with polyisocyanates.[12]

Experimental

Measurement

The ^1H NMR spectra were taken on a Brucker AC 250 (250 MHz) and JEOL-FX 100 (100 MHz) spectrometers in $CDCl_3$. The chemical shifts are given in parts per million downfield from tetramethylsilane (TMS) as the internal standard. The IR spectra were taken for samples in KBr pellets on a Perkin Elmer (Spectrum BX II) spectrometer. The UV spectra were recorded on a Spectronic Genesys 8 spectrometer in acetonitrile at 10^{-4} M in a microcell with an internal width of 1 mm.

Thermal transition data for the synthesized TM were collected using a TA Instruments Model 2929 Differential Scanning Calorimeter (New Castle, DE) equipped with a DSC refrigerated cooling system (–70°C minimum temperature limit), and dry helium and nitrogen exchange gases. The calorimeter ran on a Thermal Analyst 2100 workstation with version 8.10B software. An empty aluminium pan was used as the reference. The samples were prepared by placing 4 to 12 mg of neat charge transport material into an aluminum sample pan and crimping the upper lid to produce a hermetically sealed sample for DSC testing. The results were normalized on a per unit mass basis. Each sample was evaluated using 10°C/min heating and cooling rates with a 5–10 min isothermal bath at the end of each heating or cooling leg. The heat and cool cycles were used to remove the thermal history of the sample, to determine the single transition for monocrystalline materials, and to determine the contribution of the first and second melting transitions of the polycrystalline charge transport material to the glass transition temperature. Monocrystalline materials were heated twice: the first heat to determine the melting transition and the second heat to identify the glass transition temperature. Polycrystalline materials were heated three times: the first heat to isolate and determine the lower temperature melting transition, the second heat to identify a glass transition produced by the melting of the lower melt transition and to determine the higher temperature melting transition, and the final heat to determine the second melting transition of the metastable glass phase. The cooling ramps were used to identify either a recrystallization exotherm or a glass transition temperature for the melted charge transport material during solidification. The melting temperature was reported as the onset of melting and the glass transition midpoint as at the inflection point obtained during the second or third heating ramps for monocrystalline or polycrystalline materials, respectively.

Ionization potential was measured by the photoemission in air method described in Refs. 10 and 13.

The branched hydrazones are able to form stable layers without binder, so samples for mobility measurements were prepared from neat TM and from 1:1 mass proportion compositions with various binders. The various types of polyvinylbutyral and polycarbonate include PVB1 from Aldrich, PVB 41,843-9 with average M_W = 70,000 – 100,000 and 18–20 wt.% of hydroxyl groups; PVB2 from Sekisui S-LEC B BX-1; PVB3 from Sekisui S-LEC B BX-5; PVB4 from Solutia PVB B-79 with average M_W = 50,000 – 70,000 and 10.5–13 wt.% of hydroxyl groups; and PC-Z from Mitsubishi Gas Chemical Co. polycarbonate Iupilon Z-200. All TM investigated here form transparent layers with these binders. The samples for mobility measurements were prepared by coating TM solutions or solutions of the TM compositions with binder in THF on polyester film with a conductive Al layer. The coated samples were heated at 80°C for 2 h to dry. The layer thickness was in the range 5–10 μm. The crosslinked samples were prepared from a composition comprising TM, PVB1 and polyisocyanate Desmodur L75 of Bayer AG (DEL) in wt. proportion 70:15:15. The samples were heated at 120°C for 0.5 h to crosslink.

The hole drift mobility was measured by xerographic time of flight (XTOF) technique.[14–16] Positive corona charging created an electric field inside the TM layer. The charge carriers were generated at the layer surface by illumination with pulses of nitrogen laser (pulse duration was 2 ns, wavelength 337 nm). The layer surface potential decrease as a result of pulse illumination was up to 1–5% of the initial potential before illumination. The capacitance probe that was connected to the wide frequency band electrometer measured the speed of the surface potential decrease, dU/dt. The transit time t_t was determined by the kink on the curve of the dU/dt transient in linear or double logarithmic scale. The drift mobility was calculated from the formula $\mu = d^2/U_0 t_t$, where d is the layer thickness and U_0 is the surface potential at the instant of illumination

Materials

Synthesis of bis{4,4′-[6-(4-(diethylamino)benzylidene)-3-hydroxy-5-phenyl-5,6-diaza-1-thiahexyl]phenyl}sulfide (TM1). 1.75 ml (12.6 mmol) of triethylamine (TEA) were slowly added to the solution of 10.2 g (31.5 mmol) of 4-(diethylamino)bezaldehyde N-2,3-epoxypropyl-N-phenylhydrazone and 3.76 g (15.0 mmol) of 4,4‘-thiobisbenzenethiol in 25 ml of 2-butanone, while the temperature of the reaction mixture was maintained below 30°C. Then the reaction mixture was stored over night at room temperature. After evaporation of the solvent the residue was dissolved in 25 ml of toluene and cooled till –5°C. 11.0 g (81.5%) of crystalline product were filtered off and recrystallized from toluene. ^1H NMR (250 MHz, DMSO-d_6): 7.74 (s, 2H, CH = N); 7.44 (d, J = 8.5 Hz, 8H, 2-H, 3-H, 5-H, 6-H, *p*-Ph); 7.33 (d, J = 8.4 Hz, 4H, *p*-Ph′); 7.25–7.12 (m, 8H, 2-H, 3-H, 5-H, 6-H, Ph); 6.80 (t, J = 7.1 Hz, 2H, 4-H, Ph); 6.64 (d, J = 8.4 Hz, 4H, *p*-Ph′); 5.54 (d, J = 3.9 Hz, 2H, OH); 4.22–3.90 (m, 6H, NCH_2CH); 3.30 (q, J = 6.9 Hz, 8H, $C\underline{H}_2CH_3$); 3.18 (m, 4H, CH_2S); 1.06 (t, J = 7.1 Hz, 12H, $CH_2C\underline{H}_3$). IR spectrum, ν, cm^{-1}: 3434 (OH, br); 3058, 2967, 2925, 2871 (CH); 812, 744, 691 (CH = CH of mono- and *p*-disubstituted benzene). Found, %: C 69.50; H 6.61; N 9.44. $C_{52}H_{60}N_6O_2S_3$; Calculated, %: C 69.61; H 6.74; N 9.37.

Bis{4,4′-[6-(julolidine-9-ylmethylene)-3-hydroxy-5-phenyl-5,6-diaza-1-thiahexyl]phenyl} sulfide (TM2) was prepared and isolated as described for **TM1**, except that julolidine aldehyde N-2,3-epoxypropyl-N-phenylhydrazone (10.9 g, 31.5 mmol) was used instead of 4-(diethylamino)bezaldehyde N-2,3-epoxypropyl-N-phenylhydrazone. The yield of **TM2** was 10.2 g (71.8%). The product was recrystallized from toluene. ^1H NMR (100 MHz, $CDCl_3$): 7.5 (s, 2H, CH = N); 7.4–6.8 (m, 22H, Ar); 4.3 (m, 2H, CH); 3.9 (m, 4H, NCH_2); 3.6–3.0 (m,

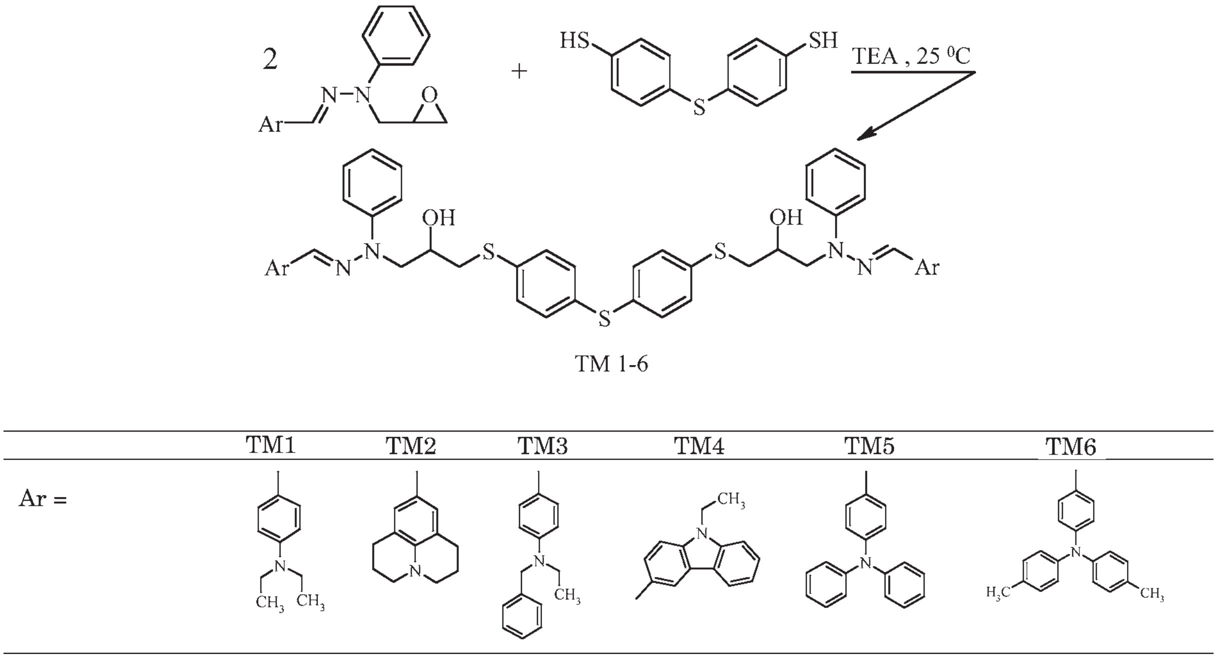

Scheme 1. Synthesis route of molecular glasses **TM1–TM6**.

10H, OH, SCH_2, $NC\underline{H}_2CH_2CH_2$); 2.7 (t, J = 6.2 Hz, 4H, $NCH_2CH_2C\underline{H}_2$); 1.9 (p, J = 5.7 Hz, 4H, $NCH_2C\underline{H}_2CH_2$). IR spectrum, ν, cm^{-1}: 3401 (OH, br); 3044, 2929, 2836 (CH); 810, 748, 692 (CH = CH of mono- and *p*-disubstituted benzene). Found, %: C 71.03; H 6.19; N 8.79. $C_{56}H_{60}N_6O_2S_3$; Calculated, %: C 71.15; H 6.40; N 8.89.

Bis{4,4′-[6-(4-(benzylethylamino)benzylidene)-3-hydroxy-5-phenyl-5,6-diaza-1-thiahexyl]-phenyl}sulfide (TM3) was prepared and isolated as described for **TM1**, except that 4-(benzylethylamino)-bezaldehyde N-2,3-epoxypropyl-N-phenylhydrazone (12.1 g, 31.5 mmol) was used instead of 4-(diethylamino)bezaldehyde N-2,3-epoxypropyl-N-phenylhydrazone. The yield of **TM3** was 10.9 g (71.2%). The product was recrystallized from toluene. ^{1}H NMR (100 MHz, $CDCl_3$): 7.5 (d, J = 8.5 Hz, 4H, Ph); 7.4–6.7 (m, 30H, Ar); 6.6 (d, J = 8.5 Hz, 4H, Ph); 4.58 (s, 4H, CH_2-Ph); 4.2 (m, 2H, $C\underline{H}OH$); 3.9 (m, 4H, $NC\underline{H}_2CH$); 3.5 (q, J = 7,3 Hz, 4H, $C\underline{H}_2CH_3$); 3.25 (s, 2H, OH); 3.1 (d, J = 6.0 Hz, 4H, CH_2S); 1.2 (q, J = 7.3 Hz, 6H, $CH_2C\underline{H}_3$). IR spectrum, ν, cm^{-1}: 3600–3250 (OH); 3050, 2970, 2920 (CH); 810, 749, 699 (CH = CH of mono- and *p*-disubstituted benzene). Found, %: C 72.79; H 6.33; N 8.29. $C_{62}H_{64}N_6O_2S_3$; Calculated, %: C 72.91; H 6.32; N 8.23.

Bis{4,4′-[6-(9-ethylcarbazol-3-ylmethylene)-3-hydroxy-5-phenyl-5,6-diaza-1-thiahexyl]phenyl}sulfide (TM4) was prepared and isolated as described for **TM1**, except that 9-ethyl-3-carbazolecarboxaldehyde N-2,3-epoxypropyl-N-phenylhydrazone (11.6 g, 31.5 mmol) was used instead of 4-(diethylamino)bezaldehyde N-2,3-epoxypropyl-N-phenylhydrazone. The yield of **TM4** was 11.7 g (79.0%). The product was recrystallized from chlorobenzene. ^{1}H NMR (250 MHz, DMSO-d_6): 8.28 (s, 2H, 4-H of carbazole); 8.18 (d, J = 7.9 Hz, 2H, 1-H of carbazole); 8.03 (s, 2H, CH = N); 7.85 (d, 2H, 2-H of carbazole); 7.60–7.10 (m, 24H, Ar); 6.85 (t, J = 6.5 Hz, 2H, 4-H_{Ph}); 5.59 (d, 2H, OH); 4.40 (q, J = 6.9 Hz, 4H, $C\underline{H}_2CH_3$); 4.30–4.0 (m, 6H, NCH_2CH); 3.30–3.10 (m, 4H, CH_2S); 1.30 (t, J = 7.0 Hz, 6H, $CH_2C\underline{H}_3$). IR spectrum, ν, cm^{-1}: 3620–3200 (OH); 3054, 2975, 2930 (CH); 810, 749, 694 (CH = CH of carbazole, mono- and *p*-disubstituted benzene). Found, %: C 72.79; H 6.33; N 8.29. $C_{62}H_{64}N_6O_2S_3$; Calculated, %: C 72.91; H 6.32; N 8.23.

Bis{4,4′-[6-(4-(diphenylamino)benzylidene)-3-hydroxy-5-phenyl-5,6-diaza-1-thiahexyl]-phenyl}sulfide (TM5) was prepared as described for **TM1**, except that 4-(diphenylamino)bezaldehyde N-2,3-epoxypropyl-N-phenylhydrazone (13.2 g, 31.5 mmol) was used instead of 4-(diethylamino)bezaldehyde N-2,3-epoxypropyl-N-phenylhydrazone. The crystals formed upon standing of the reaction mixture were filtered off and washed with 2-propanol to give 11.6 g (70.9%) of compound **TM5**. The product was recrystallized from toluene. ^{1}H NMR (250 MHz, $CDCl_3$): 7.54 (s, 2H, CH = N); 7.45 (d, J = 8.5 Hz, 4H, Ar); 7.37–6.86 (m, 42H, Ar); 4.20 (m, 2H, CH); 4.01 (m, 4H, NCH_2); 3.18 (dd, H_A of ABX, SCH_2; J_{AB} = 13.7 Hz, J_{AX} = 5.5 Hz); 3.09 (dd, H_B of ABX, SCH_2; J_{BX} = 6.8 Hz). 3.00/d, g=3.3 Hz, H,OH IR spectrum, ν, cm^{-1}: 3414 (OH, br); 3067, 3033, 2914 (CH); 819, 751, 695 (CH = CH of mono- and *p*-disubstituted benzene). Found, %: C 74.79; H 5.39; N 7.59. $C_{68}H_{60}N_6O_2S_3$; Calculated, %: C 74.97; H 5.55; N 7.71.

Bis{4,4′-[–6-(4-(4,4′-dimethyldiphenylamino)benzylidene)-3-hydroxy-5-phenyl-5,6-diaza-1-thiaheyl]phenyl}sulfide (TM6) was prepared and isolated as described for **TM1**, except that 4-(4,4′-dimethyldiphenylamino)benzaldehyde N-2,3-epoxypropyl-N-phenylhydrazone (14.1 g, 31.5 mmol) was used instead of 4-(diethylamino)bezaldehyde N-2,3-epoxypropyl-N-phenylhydrazone. The yield of **TM6** was 13.5 g (78.5%). The product was recrystallized from toluene. ^{1}H NMR spectrum (250 MHz, CDCl3): 7.53 (s, 2H, CH = N); 7.43–6.95 (m, 42H, Ar); 4.19 (m, 2H, CH); 4.03 (dd, 2H, NCH_2, H_A of system ABX, J_{AB} = 15.0 Hz; J_{AX} = 4.1 Hz); 3.95 (dd, 2H, NCH_2, H_B of system ABX, J_{BX} = 7.7 Hz); 3.17 (dd, 2H, SCH_2, H_A of system ABX, J_{AB} = 14.9 Hz; J_{AX} = 5.9 Hz); 3.09 (dd, 2H, SCH_2, H_B of system ABX,

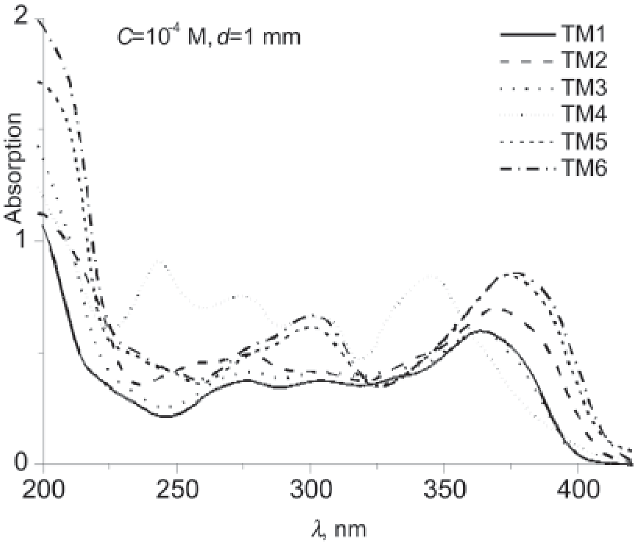

Figure 1. UV absorption spectra of the solutions of **TM1-6** in CH_3CN.

TABLE I. Glass Transition Temperature (T_g), Melting Points (T_m) and Ionization Potential I_p of TM1-TM6.

Compound	T_{m1}*, °C	T_{g1}*, °C	T_{m2}†, °C	T_{g2}†, °C	I_P (eV)
TM1	155	54	—	—	5.10
TM2‡	94	71	120	75	5.03
TM3	118	51	—	—	5.24
TM4‡	147	78	184	84	5.38
	(recry. 149, 23%)§	very weak	(recry. 137, 6%)¶		
TM5‡	134	82	188	83	5.34
TM6‡	83	85	126	83	5.21

* T_m of the crystal with the lowermost melting point.
† T_m of the crystal with the highest melting point.
‡ Exibits polymorphism.
§ Recrystallization exothermic transition during cooling
¶ Recrystallization exothermic transition during heating

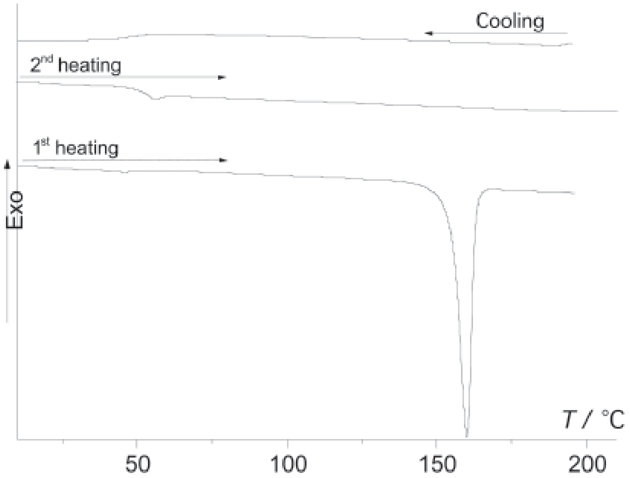

Figure 2. DSC curves of **TM1** (heating and cooling rate 10°C/min).

J_{BX} = 7.0 Hz); 3.07(s, 2H, OH); 2.31 (s, 12H, CH_3). IR spectrum, ν, cm^{-1}: 3600–3200 (OH); 3024, 2917, 2862 (CH); 814, 749, 693 (CH = CH of mono- and *p*-disubstituted benzene). Found, %: C 75.30; H 5.75; N 7.15. $C_{72}H_{68}N_6O_2S_3$. C 75.49; H 5.98; N 7.34.

Results and Discussion

The general route to the branched hydrazone derivatives including diethylaniline (**TM1**), julolidine (**TM2**), benzylethylaniline (**TM3**), ethylcarbazole (**TM4**), triphenylamine (**TM5**) and dimethyltriphenylamine (**TM6**) moieties is shown in the Scheme 1. These compounds were prepared by the reaction of 4,4′-thiobisbenzenethiol with 2 equivalents of corresponding arylaldehyde or hetarylaldehyde phenylhydrazone *N*-2,3-epoxypropyl derivative in the presence of catalyst TEA. The branched hydrazones synthesized with a flexible central thiophenyl sulfide containing bridge have been found to exhibit glass transition phenomena usually associated with polymers. In contrast to amorphous polymers the branched hydrazones are pure materials with well-defined molecular structures and definite molecular weights without any distribution. They were identified by IR, UV, NMR spectroscopy and elemental analysis.

In the ^{1}H NMR spectra the peaks of aromatic protons of all synthesized TM are in 8.30–6.6 ppm region, while the aliphatic protons appears in the region of 4.6–1.0 ppm. The doublet of OH group at 5.6–5.4 ppm in the ^{1}H NMR spectra recorded in DMSO-D_6 solutions confirmed the nucleophilic opening of the oxirane ring at the primary carbon atom. In addition, the IR spectra exhibit a broad absorption band in the 3620–3200 cm^{-1} region, which demonstrates strong hydrogen bonding in the synthesized TM. The largest shift of absorption to longer wavelengths due to conjugated π-electrons were observed in UV spectra (Fig. 1) for branched hydrazones with triphenylamine moieties (**TM5**, **TM6**). On the other hand, julolidine containing hydrazone (**TM2**) exhibits bathochromic shift compared with branched hydrazones containing diethylaniline (**TM1**), benzylethylaniline (**TM3**) and ethylcarbazole (**TM4**) chromophores.

Table I lists the melting and glass transition temperatures for the TM in this study. The formation of the glassy state in **TM1–TM6** was confirmed by differential scanning calorimetry. As an example of a monocrystalline material, Fig. 2 shows the first and second DSC heating cycles for **TM1**. The **TM1** sample, obtained by recrystallization from toluene, produced an endothermic melting transition at 155°C during the first heating cycle and did not subsequently recrystallize when cooled at a comparatively slow rate of 10°C/min. It exhibited a glass transition temperature of 54°C during the heating leg of the second cycle. The absence of an exothermic recrystallization transition indicates that this material formed a metastable glass phase during the time period of this thermal investigation. This is a common feature for all of the investigated TM, with the exception of **TM4**.

The presence of rigid N-ethylcarbazolyl groups in **TM4** increased the T_g by 30°C over the T_g of **TM1**. A very weak T_g was observed at 78°C during the second heating cycle that was not visible during the third heating cycle (Fig. 3). Also, two small exothermic transitions were observed.

The onset temperatures for the exothermic transitions occurred at 149°C and 137°C during the first cooling and the subsequent heating legs, respectively. If these exothermic transitions were the result of recrystallization of the material phase that melted at 147°C during the first heat leg then these cooling and heating exotherms represents 23% and 6% recrystallization of

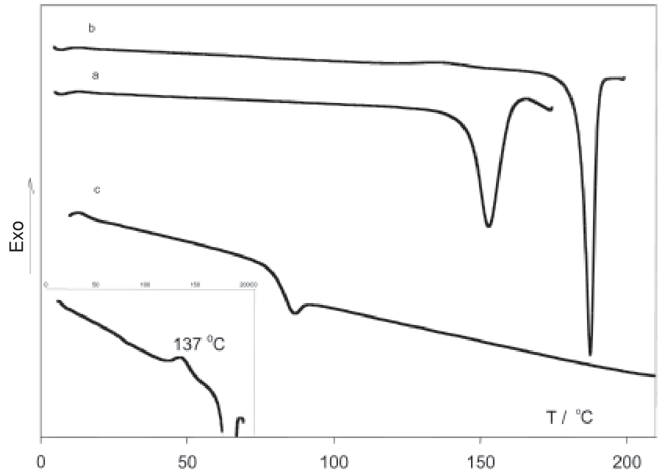

Figure 3. DSC curves of **TM4**. Curve (a) is for the first heating through the lower melt transition, curve (b) is for the second heating through the second melt transition, and curve (c) is for the third heating. The insert shows the recrystallization exotherm from curve (b).

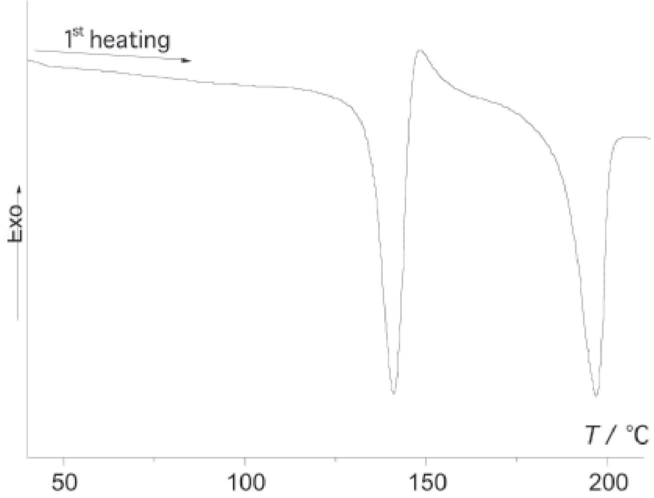

Figure 4. DSC curve of **TM5** (first heating through first and second melting transitions, rate 10°C/min).

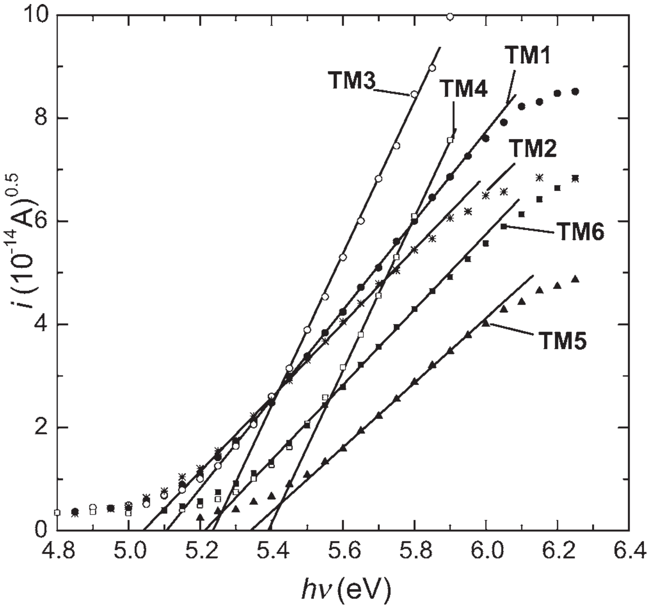

Figure 5. Photoelectron emission spectra in air of **TM1**–**TM6**.

the melted material at 147°C, respectively. No subsequent exothermic transitions (recrystallizations) were observed following the melting of the second transition at 184°C, i.e., no exothermic transitions were observed during the second cooling or the third heat legs.

In other observations, the T_g increased as the molecular size and weight of the TM increased (compare **TM1** with **TM4** and **TM5** with **TM6**), and branched hydrazones **TM2**, **TM4–TM6**, displayed polymorphism. For example, Fig. 4 shows the DSC curve of the two different crystal forms of **TM5** with melting points at 134°C and 187°C.

The photoelectron emission in air spectra for the investigated TM are given in Fig. 5; the ionization potential values are presented in Table I. The lowest values of the ionization potential are for the **TM2** and **TM1** with julolidine and diethylaniline groups; the largest values are for **TM4** and **TM5** with carbazole or triphenylamine groups. Ionization potential shows a tendency to decrease with increasing number of aliphatic substituents.

XTOF measurements revealed that small charge transport transients are Gaussian with well-defined transit time on linear or log–log plots in all the cases investigated, both for the samples of pure TM or compositions with various binders. This is illustrated in Figs. 6 and 7. Examples of mobility field dependencies are given in Fig. 8. In all the cases mobility μ may be adequately approximated by the formula

$$\mu = \mu_0 \exp\left(\alpha\sqrt{E}\right). \qquad (1)$$

where μ_0 is the zero field mobility, α is Pool–Frenkel parameter and E is electric field strength. The mobility defining parameters μ_0 and α values as well as the mobility value at the 6.4×10^5 V/cm field are given in Table II.

As seen from the results presented the mobility value is influenced by the nature of the charge transporting chromophore. The highest mobility values are for chromophores based on triphenylamine (**TM5**) and dimethyltriphenylamine (**TM6**) moieties. This is reasonable because the conjugated π electron systems are the largest in these chromophores. Aliphatic groups attached directly to the chromophore lead to increased mobility. However, chromophore size does not always seem to be the decisive factor determining mobility. The chromophore of **TM4** with a carbazole ring is as large as the chromophore of **TM1** with diethylaniline. However, mobility is higher in **TM1**. It is necessary to note that mobility in the TM investigated as well as compositions of them with binders is large enough for practical application in many cases. Mobility may also be gained using a low concentration of binders, which is possible with these TM.

Mobilities in compositions of TM with binders are considerably lower compared with those in neat TM. The difference may be up to two orders of magnitude. The highest mobility among the **TM5** compositions, as one can see from Fig. 8 and Table II, is in the case of poly-

TABLE II. Mobility Data for Neat TM and Compositions with Binder Materials.

Layer composition	μ_0 (cm^2/V·s)	μ (cm^2/V·s)	α (cm/V)$^{0.5}$
TM1	2.2×10^{-7}	2.3×10^{-5}	0.0058
TM1+PVB1, 1:1	1.2×10^{-8}	1.6×10^{-6}	0.0061
TM2	6.0×10^{-8}	4.7×10^{-6}	0.0054
TM2+PVB1, 1:1	2.9×10^{-9}	2.4×10^{-7}	0.0055
TM3	3.8×10^{-7}	1.7×10^{-5}	0.0048
TM3+PVB1, 1:1	1.3×10^{-8}	5.8×10^{-7}	0.0048
TM4	1.3×10^{-7}	1.3×10^{-5}	0.0058
TM4+PVB1, 1:1	2.8×10^{-9}	5.2×10^{-7}	0.0065
TM5	5×10^{-6}	2.6×10^{-4}	0.0050
TM5+PVB1, 1:1	4.6×10^{-8}	1.5×10^{-6}	0.0044
TM5+PVB2, 1:1	5.5×10^{-8}	2.0×10^{-6}	0.0045
TM5+PVB3, 1:1	5.8×10^{-8}	1.8×10^{-6}	0.0043
TM5+PVB4, 1:1	6.3×10^{-8}	2.5×10^{-6}	0.0046
TM5+PC-Z, 1:1	1.7×10^{-7}	4.9×10^{-6}	0.0042
TM6	9.0×10^{-6}	4.7×10^{-4}	0.0049
TM6+PVB1, 1:1	1.8×10^{-7}	7.6×10^{-6}	0.0047

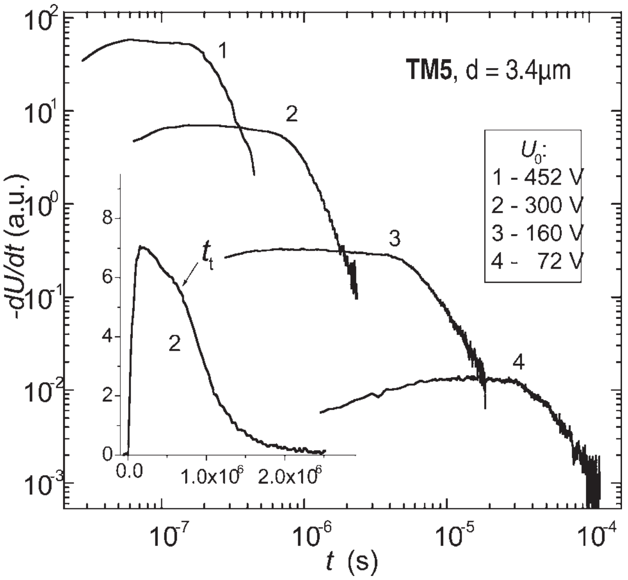

Figure 6. XTOF transients for pure **TM5**. Insert shows a typical transient curve in linear plot.

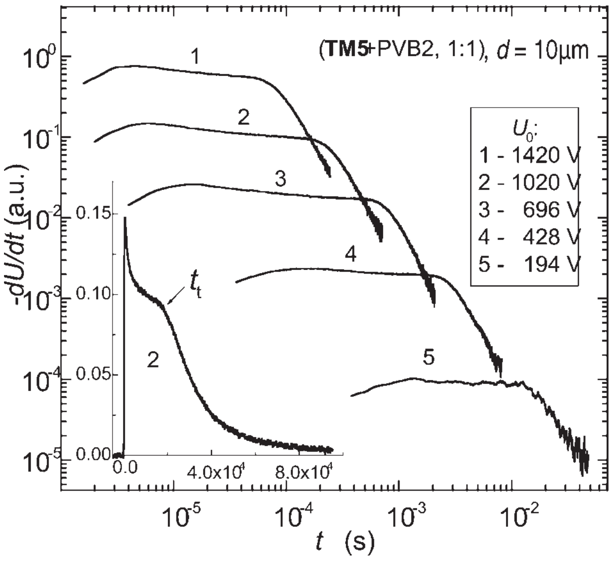

Figure 7. XTOF transients for **TM5** 1:1 composition with PVB2.

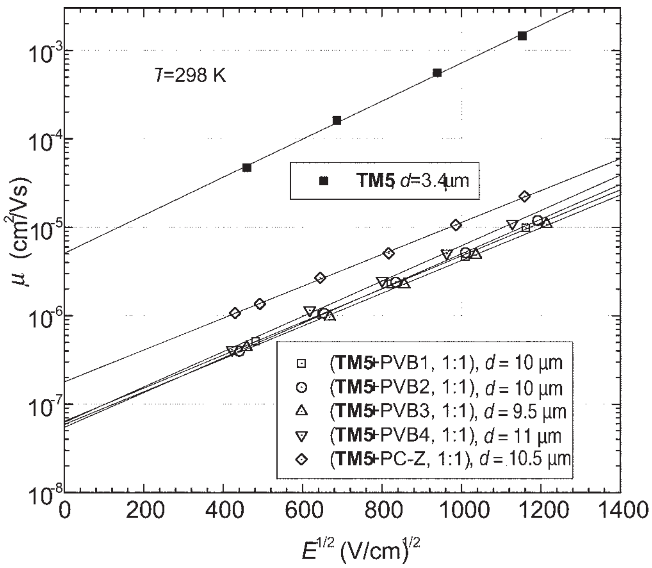

Figure 8. Mobility field dependencies for pure **TM5** and its 1:1 compositions with various binders.

carbonate binder. Mobility in this case is higher by a factor of about 2–2.5 compared with various sorts of PVB. The hydroxyl groups present in PVB probably cause this. However, special properties of PVB due to presence of hydroxyl groups, such as good adhesion, stability to bending, stretching, and effects of liquid developer may outweigh loss of mobility.

While presence of binder in the TM layer reduces mobility considerably, it has little effect on the mobility field dependence. This is seen from mobility field dependencies presented in Fig. 8 and in Table II, where the field dependence defining parameter α is given. In the case of **TM4** and some others, the parameter α is somewhat larger in the presence of binder, but in some other cases, as with **TM5**, it is even smaller in TM compositions with binder compared with neat TM. According to widely used charge transport models for molecularly doped polymers mobility and its field dependence are determined by the energetic and positional disorders in the transporting composition. The mobility data in the molecular solids are usually interpreted in terms of the following formula, proposed by Borsenberger, Pautmeier and Bässler[17]:

$$\mu(E,T) = \mu_0'\exp\left[-\left(\frac{2\sigma}{3kT}\right)^2\right]\exp\left\{C\left[\left(\frac{2\sigma}{3kT}\right)^2 - \Sigma^2\right]E^{1/2}\right\}. \quad (2)$$

where, μ is the mobility, σ is the energy width of the hopping site manifold, which provides a measure of the energetic disorder, Σ is the degree of positional disorder, E the electric field, μ_0' is a mobility pre-factor, C is an empirical constant of 2.9×10^{-4} (cm/V)$^{1/2}$ and kT has its usual meaning. It is evident from this formula that the zero field mobility $\mu(0,T)$ is determined by the ener-

TABLE III. Hole Mobility Data for Crosslinked Compositions.

Layer composition	μ_0 (cm²/V·s)	μ (cm²/V·s)	α (cm/V)$^{0.5}$
TM1+PVB1+DEL, 70:15:15	5.0×10^{-9}	1.0×10^{-6}	0.0065
TM4+PVB1+DEL, 70:15:15	1.6×10^{-9}	6×10^{-7}	0.0074
TM5+PVB1+DEL, 70:15:15	1×10^{-7}	1.9×10^{-6}	0.0037
TM6+PVB1+DEL, 70:15:15	1.8×10^{-7}	4×10^{-6}	0.0038

getic disorder σ, while mobility field dependence is caused by the difference between the energetic disorder σ and positional disorder Σ dependent terms in the formula. As seen from Eq. (2) the energetic disorder σ increases and the positional disorder Σ decreases the mobility field dependence.

We had an opportunity to investigate mobility both in neat TM and compositions of these materials with binder materials. To interpret our experimental data we assume that introduction of BM leads to an increase of both of energetic and positional disorders so, that the difference

$$\Delta = (2\sigma / 3kT)^2 - \Sigma^2 = \alpha / C \tag{3}$$

in Eq. (2) remains little changed despite considerable change of both terms. The difference between the terms of energetic and positional disorder for various TM is also not correlated with mobility vales. So mobility in **TM2** and **TM6** differ by two orders of magnitude, but the parameter α values are close. An increase of the positional disorder with introduction of binder material into the composition is understandable. Presence of binder material leads to an increase of distance between TM molecules, the binder material intervening between a TM molecule and its nearest neighbor may be different for different pairs of molecules. However, in the case of pure TM the molecules are in close contact with each other, so distances between different pairs of neighbor molecules may not vary much. One of the assumptions behind Eq. (2) is that location of particular hopping site is independent of locations of other sites.[18] This may be true in the case where hopping site size is much less than the distances between sites, as it is, for example, with atomic impurities in crystalline semiconductors. In the case of neat TM however, distances between the nearest molecules are essentially the same as molecular dimensions, the molecules are in contact with each other and it is not obvious what may be the meaning of positional disorder in neat TM.

The zero field mobility, according to Eq. (2), is determined by the energetic disorder. It follows from the results presented that energetic disorder increases with introduction of binder material into TM. This suggests that the molecular energy levels are changed by the presence of binder material. Again it is not clear how this happens: how molecular structure of charge transporting chromophores and presence of specific atom groupings in them effects energetic disorder. Differences of zero field mobility between various TM, both neat or with binder material, are significant, so differences between energetic disorder parameters σ should also be big. However, existing charge transport theories do not take into account molecular structure of TM and spectral or other characteristics of TM.

Dunlap, Kenkre and Paris[19] proposed another charge carrier transport model in organic transporting media which yields Poole–Frenkel type field dependence as described by Eq. (1). There is no positional disorder in this model and energetic disorder is considered as correlated disorder, originally defined by Novikov and Vannikov.[20] Energetic disorder is considered as presence of continuous "hills" and "valleys" caused by the action of impurities with dipole moments. There are no abrupt energy level thresholds between the neighbor molecules. The expression for mobility is[19]

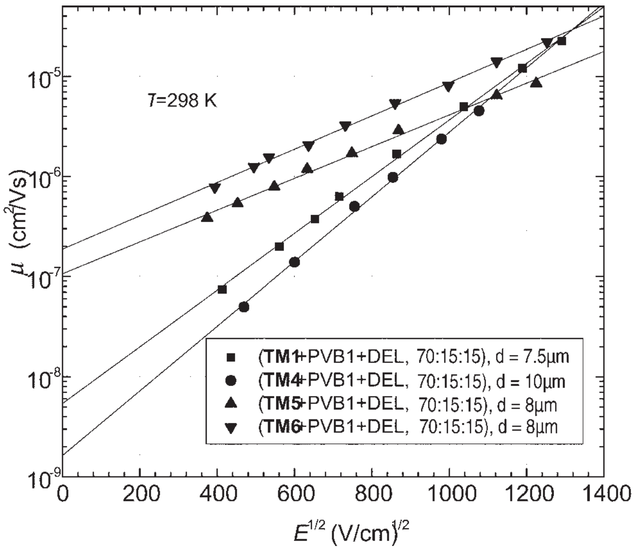

Figure 9. Hole mobility field dependencies in crosslinked compositions.

$$\mu = \mu_0 \exp\left[-(\sigma / kT)^2 + \gamma E^{1/2}\right], \tag{4}$$

$$\gamma = \left[4\sigma^2 ea / (kT)^3\right]^{1/2}. \tag{5}$$

where a is scaling factor of the magnitude close to intermolecular distances. This model gives new opportunities to interpret mobility data in organic transporting compositions. Usually there is large concentration of polar groups in transporting compositions. Charge transporting chromophores have their own dipole moments. For example compounds **2** and **10** in Ref. 21 are close analogs of the chromophores of **TM4** and **TM5** investigated here. The dipole moments of these compounds are 2.57 and 2.35D respectively.[21] There are polar hydroxyl groups in the central connecting bridges of the TM investigated here. Polar groups are also present in binder materials, polycarbonate and polyvinylbutiral, so concentration of polar groups in the TM and transporting compositions investigated here is high, and this may be an important factor determining properties of organic transporting materials.

The XTOF transients for the crosslinked samples were of disperse character but transit time were obtained from log–log plots. The hole mobility measurement results for crosslinked compositions are presented in Fig. 9 and in Table III. The mobility values at strong electric field, as a rule, are close to the values in the compositions with PVB. However, concentration of TM in the uncrosslinked compositions is 50 wt.% while it is 70 wt.% in crosslinked compositions. This means that crosslinking is affecting mobility more than does simple admixture of BM. Mobility field dependence for **TM1** and **TM4** is somewhat stronger and for **TM5** and **TM6** weaker in crosslinked compositions.

Conclusions

A series of new glass-forming hydrazones **TM1–TM6** containing diethylaniline, julolidine, benzylethylaniline, ethylcarbazole, triphenylamine and dimethyltriphenylamine moieties have been synthesized by the reaction of 4,4‘-thiobisbenzenethiol with N-2,3-epoxypropyl derivative of phenylhydrazone of corresponding aromatic aldehyde in the presence of triethylamine. The molecular structure of these branched hydrazones prevents transporting material crystallization in the layer and allows stable films to be prepared even without binder material or at low concentration thereof. These TM are accordingly compatible not only with traditional binder material, e.g., polycarbonate but also with polyvinylbutyral. The hydroxyl groups allow crosslinking these transporting materials in the layer. The hole mobility of both neat **TM1–TM6** and compositions of them with binder materials have been studied. The highest hole mobility, reaching 10^{-4} cm^2/Vs at 6×10^5 V/cm electric field, was observed in the TM with dimethyltriphenylamine or triphenyl-amine moieties. It is about one order of magnitude higher than in diethylaniline, benzylethylaniline or ethylcar-bazole moiety containing materials and about two orders of magnitude higher than in the julolidine chromophore containing TM.

References

1. N. Mori, US Patent 5,567,557 (1996).
2. N. Tatsya and U. Minoru, Japan Patent 8,101,524 (1996).
3. Y. Suzuki, US Patent 5,665,500 (1997).
4. N. Jubran, Z. Tokarski and T. P. Smith, U.S. Patent 6,340,548 (2002).
5. S. Nomura and K. Nishimura, *Thin Solid Films* **273**, 27 (1996).
6. H. Nam, D. H. Kang, J. K. Kim, and S. Y. Park, *Chem Lett.* 1298 (2000).
7. P. M. Borsenberger, *Adv. Chem. Mater. Opt. Electr.* **1**, 73 (1992).
8. S. Nomura, K. Nishimura and Y. Shirota, *Mol. Cryst. Liq. Cryst.* **313**, 247 (1998).
9. S. Kutkevicius, A. Stanisauskaite, V. Getautis, and A. Railaite, *J. Prakt. Chem.* **337**, 315 (1995).
10. M. Daskeviciene, V. Gaidelis, V. Getautis, V. Jankauskas, O. Paliulis, and J. Sidaravicius. *Lithuanian J. Physics* **41**, 4–6, 521 (2001).
11. M. Daskeviciene, V. Getautis, J. V. Grazulevicius, A. Stanisauskaite, J. Antulis, V. Gaidelis, V. Jankauskas, and J. Sidaravicius, *J. Imaging Sci. Technol.* **46**, 467–472 (2002).
12. V. Gaidelis, J. Gavutiene, V. Getautis, J. V. Grazulevicius, V. Jankauskas, R. Kavaliunas, R. Lazauskaite, O. Paliulis, M. A. Rossman, D. J. Sidaravicius, T. P. Smith, and A. Stanisauskaite, US Patent 6,214,503, (2001).
13. S. Grigalevicius, G. Blazys, J. Ostrauskaite, J. V. Grazulevicius, V. Gaidelis, V. Jankauskas, and E. Montrimas, *Synthetic Metals* **128**, 127 (2002).
14. E. Montrimas, V. Gaidelis and A. Pazera. *Lithuanian Journal of Physics* **6**, 569 (1966).
15. S. M. Vaezi-Nejad, *Intl. J. Electronics* **62**, 361–384 (1987).
16. A. Y. C. Chan and C. Juhasz, *Intl. J. Electronics*, **62**, 625–632 (1987).
17. P. M. Borsenberger, L. Pautmeier and H. Bässler, *J. Chem. Phys.* **94**, 5447–5454 (1991).
18. P. Borsenberger and D. Weiss, *Organic Photoreceptors for Xerography*, Marcel Dekker, Inc., 1998, p. 326.
19. D. H. Dunlap, V. M. Kenkre and P. E. Paris, *J. Imaging Sci. Technol.* **43**, 432 (1999).
20. S. V. Novikov and A. V. Vannikov, *Synth. Met.* **85**, 1167 (1997).
21. A. Fuji, T. Shoda, S. Aramaki, and T. Murayama, *J. Imaging Sci. Technol.* **43**, 430 (1999).